ECOSYSTEM ECOLOGY – ORIGINAL RESEARCH

CrossMark

Landscape variation in canopy nitrogen and carbon assimilation in a temperate mixed forest

Zaixing Zhou[1] · Scott V. Ollinger[1] · Lucie Lepine[1]

Abstract

Canopy nitrogen (N) is a key factor regulating carbon cycling in forest ecosystems through linkages among foliar N and photosynthesis, decomposition, and N cycling. This analysis examined landscape variation in canopy nitrogen and carbon assimilation in a temperate mixed forest surrounding Harvard Forest in central Massachusetts, USA by integration of canopy nitrogen mapping with ecosystem modeling, and spatial data from soils, stand characteristics and disturbance history. Canopy %N was mapped using high spectral resolution remote sensing from NASA's AVIRIS (Airborne Visible/Infrared Imaging Spectrometer) instrument and linked to an ecosystem model, PnET-II, to estimate gross primary productivity (GPP). Predicted GPP was validated with estimates derived from eddy covariance towers. Estimated canopy %N ranged from 0.5 to 2.9% with a mean of 1.75% across the study region. Predicted GPP ranged from 797 to 1622 g C m^{-2} $year^{-1}$ with a mean of 1324 g C m^{-2} $year^{-1}$. The prediction that spatial patterns in forest growth are associated with spatial patterns in estimated canopy %N was supported by a strong, positive relationship between field-measured canopy %N and aboveground net primary production. Estimated canopy %N and GPP were related to forest composition, land-use history, and soil drainage. At the landscape scale, PnET-II GPP was compared with predicted GPP from the BigFoot project and from NASA's MODIS (Moderate Resolution Imaging Spectroradiometer) data products. Estimated canopy %N explained much of the difference between MODIS GPP and PnET-II GPP, suggesting that global MODIS GPP estimates may be improved if broad-scale estimates of foliar N were available.

Introduction

The availability of nitrogen (N) represents a key constraint on carbon cycling in terrestrial ecosystems and serves as a useful indicator of ecosystem metabolism. The importance of N as a regulator of carbon (C) assimilation is well established through the widely observed relationship between leaf-level photosynthetic capacity (Amax) and foliar N

✉ Zaixing Zhou
zaixing.zhou@unh.edu

[1] Earth Systems Research Center, Institute for the Study of Earth, Oceans, and Space, University of New Hampshire, Durham, NH 03824, USA

concentrations (Reich et al. 1999a; Wright et al. 2004). At the canopy and stand level, canopy N concentration (%N) has been related to canopy photosynthetic capacity (Ollinger et al. 2008), plant respiration (Reich et al. 2008), net primary production (NPP) (Smith et al. 2002; Ollinger and Smith 2005; LeBauer and Treseder 2008; Reich 2012), and canopy light use efficiency (Green et al. 2003; Kergoat et al. 2008; Ollinger et al. 2008).

Canopy N status has also been linked to the availability of N in soils through mechanisms involving litter decay (Parton et al. 2007), net mineralization (Ollinger et al. 2002b), plant N uptake, and N loss (McNeil et al. 2007; Merilä and Derome 2008). The relationship between canopy N and soil N availability is important because humans have greatly altered the N cycle globally (Galloway et al. 2004), and because natural disturbance can also leave long-term legacies on vegetation (Foster 1988; Weishampel et al. 2007) and soils (McNulty 2002). Over the past several centuries, most northeastern US forests have experienced human-induced

disturbances such as forest harvests, fire, or agriculture (Foster 1992). These disturbances have had long-term impacts on forest carbon and nitrogen cycling (Aber and Driscoll 1997) and have left imprints on present-day species composition, biomass, foliar N (%), soil C and N pools (Hooker and Compton 2003), net N mineralization and nitrification (Ollinger et al. 2002b), and nitrate leaching (Goodale and Aber 2001).

Despite its central role in C cycle processes, canopy %N has been involved in a limited number of broad-scale analyses. This is partly because, until recently, methods for mapping canopy %N were largely limited to landscape scales (e.g., Ollinger and Smith 2005). However, generalizable methods for estimating canopy %N with imaging spectroscopy (Martin et al. 2008), as well as methods that use NIR reflectance from broadband sensor data to derive canopy %N, have expanded the potential to map %N across broader ranges of ecosystems at regional scales (Ollinger et al. 2008; Ollinger 2011; Lepine et al. 2016). Nevertheless, remotely sensed canopy %N has rarely been used to evaluate broader scale C cycle analyses that lack explicit treatment of canopy %N.

In this study, we conducted an analysis to examine landscape variation of canopy nitrogen and carbon assimilation in a temperate mixed forest at the Harvard Forest (HF), in Massachusetts, USA. We integrated plot-level field observations, eddy covariance (EC) data, remote sensing, and ecosystem modeling. We aimed to examine whether spatial patterns of canopy %N at the landscape scale (1) reflect patterns of local disturbance history and other available spatial data layers, and (2) are related to patterns observed in field-measured forest productivity. We also compared results with C assimilation estimates from two models that lack explicit treatment of canopy %N to assess the degree to which N mapping capabilities might benefit C cycle models more broadly.

Materials and methods

Study site

The area studied was a 10 km × 16 km landscape surrounding the Harvard Forest (HF) in central Massachusetts, USA, centered near 42.54°N, 72.19°W (Supplementary Fig. S1). It covered eight of nine research tracts maintained by HF with elevations ranging from 158 to 421 m with a median of 317 m and the average slope of 4.4°. The climate is cool and moist with July mean temperature 20 °C, January mean temperature − 7 °C, and annual mean precipitation 110 cm, distributed evenly throughout the year. The soils are mainly sandy loam glacial, with some alluvial and colluvial

deposits, and moderately to well drained in most areas (Foster 1992; Urbanski et al. 2007).

The study area is predominantly covered by a temperate mixed forest representing the transition hardwood—white pine (*Pinus strobus*)—hemlock (*Tsuga canadensis*) vegetation zone of central New England. Deciduous species are primarily Northern red oak (*Quercus rubra*), red maple (*Acer rubrum*), and black birch (*Betula lenta*). White spruce (*Picea glauca*), red pine (*Pinus resinosa*), and Norway spruce (*Picea abies*) are also present (Foster 1992).

The study area has been subjected to a complex array of historic agricultural and logging treatments as well as natural disturbances (Foster 1992). It has undergone several transformations in response to changes in land-use practices and population density since its initial settlement in the 1730s. Forest clearing to provide pasture for beef cattle and sheep resulted in an increase in open land from approximately 50% in 1800 to nearly 85% in 1850. Remaining forests occupying steep and rocky slopes, wetlands or narrow valleys were cut for timber, fuelwood, and tanbark and sometimes grazed. After the mid-1800s, farms were abandoned, followed by a period of reforestation, which continued through the early twentieth century. In addition to various land-use practices, the Harvard Forest tracts have been exposed to a wide range of natural disturbances, including wind, fire, ice, snow, and pathogen disturbances (Foster et al. 1997). The most devastating in recent history was the 1938 New England hurricane which led to a reduction of approximately 70% of the standing timber volume (Foster 1988).

PnET-II model description and data inputs

PnET-II (Aber et al. 1995; Ollinger and Smith 2005) is a daily-to-monthly time step forest ecosystem model, initially developed for the northeastern US, but later applied and validated in many temperate forest systems. The model predicts the photosynthetic capacity of forest canopies using the relationship between leaf photosynthetic capacity and leaf nitrogen (Reich et al. 1999a; Wright et al. 2004), combined with information about climate, site variables, and other plant traits. Transpiration linking soil water availability and canopy photosynthesis by water-use efficiency is regulated by atmospheric CO_2 concentration and vapor pressure deficit. Although PnET-II has a dynamic link between the fluxes of carbon and water, it lacks dynamic interactions between C and N cycles, which is incorporated into a later version, PnET-CN (Aber et al. 1997). Instead, PnET-II uses foliar %N as an input to integrate the combined effect of soil N status and species composition.

PnET-II requires a number of input parameters to describe vegetation and site characteristics, along with climate forcing data. Vegetation parameters include foliar %N, leaf mass per unit area (LMA), leaf retention time and growing-degree

day variables describing the phenology of leaf production and senescence. Vegetation parameters (Supplementary Table S1) other than foliar %N for deciduous and evergreen stands in this study followed Ollinger and Smith (2005). Required climatic and environmental inputs include average maximum and minimum temperature, precipitation, photosynthetically active radiation (PAR), and atmospheric CO_2 concentrations. For the spatial application of PnET-II, we delineated our study area into 30 m × 30 m grid cells.

The mountain microclimate model MTCLIM (Thornton et al. 1997; Thornton and Running 1999) in conjunction with a 30-m resolution digital elevation model (DEM) was used to estimate maximum and minimum temperature, precipitation, and solar radiation for each cell. Temperature estimates at the site were based on temperatures observed at weather stations (base) and a user-supplied temperature lapse rate for daily maximum and minimum temperatures. Precipitation estimates at the site were based on the daily record of precipitation from the base, and a user-specified ratio of annual total precipitation between the site and the base. In conjunction with latitude, elevation, slope, and aspect of the site (derived from digital elevation model), total solar radiation was computed by MTCLIM based on the fact that the diurnal temperature range was closely related to the daily average atmospheric transmittance (Thornton et al. 1997). In this study, the environmental measurement station (EMS) eddy flux tower at HF was used as the base station. Measured temperature and precipitation from 1964 to 2015 were used to generate PnET-II weather data, of which data from 1992 to 2015 were from EMS tower, and the remaining from a nearby weather station (Shaler Station). Average annual precipitation and temperature lapse rates were derived using values from the Hubbard Brook Experimental Forest, New Hampshire, USA, 160 km north of HF (data not shown). Maximum temperature lapse rate was 7.1 °C per kilometer, and minimum temperature lapse was 3.7 °C per kilometer. PAR was derived from estimated total solar radiation by MTCLIM scaled by a conversion factor, which was derived in this study based on regression between EMS tower data and the predicted data (1.95). Atmospheric CO_2 concentrations were estimated as described by Ollinger et al. (2002a) for the period where measured data were not available.

Remote sensing of canopy %N

Mapped estimates of mass-based canopy N concentration (g N 100 g^{-1} dry matter, %N_e) for the study area were developed by relating field measurements of foliar %N (%N_f) to airborne imaging spectrometer data collected by the NASA's Airborne Visible/Infrared Imaging Spectrometer (AVIRIS). The AVIRIS instrument measured reflected solar radiance in 224 contiguous optical bands from 0.4 to 2.4 μm with a spectral resolution of 0.01 μm. AVIRIS was flown on August

24, 2003 over the Harvard Forest and surrounding area on an ER-2 aircraft at an altitude of 20 km, producing a spatial resolution of 18 m.

Field %N_f data collection took place within 2–3 weeks of the image acquisition. Upper canopy leaf samples were collected for the dominant and codominant species on 39 plots using shotguns. This included approximately five species per plot and from three to five trees per species. Species-level foliar N concentrations (% by mass) were weighted by the proportional abundance of each species in the canopy foliar biomass to generate plot-level canopy %N_f estimates for each plot. The plots sampled were a subset of plots established by the Bigfoot project (Turner et al. 2006b) and were selected to capture the range of forest types at HF and to facilitate comparison with field-measured productivity data collected for the Bigfoot project (Sects. "Model application", "Validation data"). Additional details on foliar sampling are described in Ollinger et al. (2008).

Relationships between plot-level spectra and field %N_f were established using partial least squares (PLS) regression. The accuracy of the resulting regression models was evaluated using an iterative cross-validation procedure in which each plot was sequentially excluded from the analysis and a canopy %N prediction was generated from the remaining samples. The best-fit model ($r^2 = 0.74$; $p < 0.001$; Supplementary Fig. S2) was applied to derive canopy %N_e across the study area. Detailed descriptions of methods for deriving canopy %N_e from AVIRIS are given elsewhere (Smith and Martin 2001; Smith et al. 2003).

Model application

PnET-II treats deciduous and evergreen stands differently in terms of parameters regulating photosynthesis, phenology, and several other ecophysiological mechanisms. Because remotely sensed data provided only a single canopy %N_e estimate for each grid cell, we needed to estimate the relative proportions of deciduous and evergreen forests as well as the foliar %N of each component for each cell. An empirical unmixing approach was used to derive these parameters from remotely sensed %N_e estimates, following methods used by Ollinger and Smith (2005). Including HF plots, we used an extended data set of 96 plots measured across New England (Martin et al. 2008) to build linear relationships between AVIRIS-predicted %N_e and the proportion of field-measured %N_f in deciduous and evergreen stands (Supplementary Fig. S3) and determined the relative proportions of deciduous and evergreen in each grid cell. If the predicted %N_e was less than 0.94, the cells were defined as 100% evergreen. Cells with predicted %N_e above 2.30 were classified as 100% deciduous. Cells with predicted %N_e between the above two values were classified as mixed with the relative proportions of deciduous and evergreen derived

by the relationships shown in Supplementary Fig. S3. Within mixed stands, measured foliar $\%N_f$ values for each forest type were also significantly and positively correlated with AVIRIS-predicted $\%N_e$ for the entire pixel (Supplementary Fig. S4). This is important for two reasons. First, it demonstrates that predicted $\%N_e$ values are driven by variation in $\%N$ within forest types and not simply by differences in forest composition. Second, it provided a means of estimating foliar $\%N$ for each forest type within pixels classified as mixed (i.e., using relationships shown in Supplementary Fig. S4). These patterns likely reflect the influence N availability in soils can have on forest composition (with deciduous species becoming increasingly dominant on rich sites) as well as the foliar N concentrations within individual species (e.g., Ollinger et al. 2002b).

PnET-II was run for each vegetation type in mixed cells, and the final output results were calculated as a weighted average of the two model runs, based on the estimated proportion of deciduous or evergreen composition (Fig. S3). The model was spun up for ten cycles using weather data from 1964 to 2015. All predicted PnET-II results from 1993 to 2015 were averaged for spatial analyses, except for validation and comparison with other products as described in Sect. "Geospatial data".

Validation data

Estimates of GPP were available from two eddy covariance towers at HF, both of which were used to validate model predictions. The environmental measurement station (EMS) eddy flux tower, located on the Prospect Hill tract of Harvard Forest (42.538° N, 72.171° W, elevation 340 m, see Supplementary Fig. S1), has a record of eddy flux measurements that began in 1991 (Munger and Wofsy 1999). The area surrounding the tower is dominated by red oak and red maple, with scattered eastern hemlock, white pine, and red pine. The stand is approximately 85–120 years old on abandoned farmland. A second flux tower, Hemlock Flux Tower (HEM), is also located on the Prospect Hill tract (42.539° N, 72.180° W, elevation 355 m, see Supplementary Fig. S1) in a mesic hemlock-dominated forest with most trees 100–200 years old on undisturbed soils. Other tree species present include red maple, black birch, red oak, and white pine. Measurements at the HEM tower started in the summer of 2004 (Munger and Hadley 2003). Eddy covariance GPP estimates were computed by the difference between net ecosystem exchange (NEE) of CO_2 and respiration (R). R was derived from nighttime NEE and scaled to full day by temperature responses determined over moving windows (Urbanski et al. 2007). Although there can be substantial uncertainties in the eddy covariance data and the flux-partitioning algorithm (Reichstein et al. 2005), these estimates still represent the best source of model validation.

For additional validation and assessment of predicted spatial patterns, we used plot-level aboveground net primary production (ANPP) and LAI data collected at 20 locations within HF as part of the BigFoot project (Turner et al. 2006b; see next section) in 2002 and 2003.

Geospatial data

Maps of environmental factors (e.g., topography and soils), forest stands, and historical land-use are available on the Harvard Forest website (Hall 2005), and were used to facilitate analysis of spatial variability in canopy $\%N_e$ and simulated GPP.

A 30-m digital elevation model (DEM) was used to derive elevation, aspect, and slope for each 30-m cell in the study area, which were combined with canopy $\%N_e$ and climate data to drive PnET-II to estimate GPP across the study domain. A forest stand map (Supplementary Fig. S5a) developed from the vegetation inventory of Harvard Forest in 1986–1993 was used to examine the relationships between forest composition and other variables. Forests were classified as hardwood (H) if 75% basal area was hardwood, softwood (S) if 75% basal area was softwood, otherwise mixed (M). We used a map of soil drainage classes for the HF research tracts (Supplementary Fig. S5b) to explore the effects of soil moisture. Soils were grouped into six classes based on drainage and moisture: excessively drained (D1), somewhat well drained (D2), well drained (D3), moderately well drained (D4), very poorly drained (D5), and peat (D6). For the Prospect Hill Tract, historical land use was derived from soil plow-horizon presence and depth, field observations, and archived land-use records. Land-use categories prior to 1850s included cultivated lands (CT), improved (IP) and unimproved pastures (UP), and primary woodlots (WL). The land-use map (Supplementary Fig. S5c) was used to examine the impact of land-use legacies on canopy $\%N_e$ and estimated GPP.

The land use data layer of Massachusetts from MassGIS (http://www.mass.gov/anf/research-and-tech/it-serv-and-support/application-serv/office-of-geographic-information-massgis/datalayers/lus2005.html) was obtained to mask nonforest portions of the study area. It was created using semi-automated methods, and based on 0.5-m resolution digital ortho imagery captured in April 2005. Land-use classes of forest and forested wetlands were extracted to mask the forested area (Supplementary Fig. S1).

Spatially distributed GPP predictions from the BigFoot Project (BigFoot 2005) and predictions from the MODIS GPP product MOD17 (Running et al. 2004; Zhao et al. 2005) at HF (Supplementary Fig. S1) were compared to predictions from this study to examine seasonal and spatial patterns. In addition, spatial patterns of GPP derived from MODIS and PnET-II were examined relative to

patterns of canopy %N_e as MODIS GPP estimates lack detailed N treatment.

The BigFoot Project was designed to provide validation of MODIS science products, including GPP and net primary production (NPP). BigFoot sites spanned a 7×7 km area around flux towers with a resolution of 25 m. The project used ground measurements, remote sensing data, and ecosystem process models (e.g., Biome-BGC) at sites representing different biomes (Reich et al. 1999b). Biome-BGC was driven by remotely sensed LAI, whereas PnET-II was driven in this study by remotely sensed canopy %N_e, although Biome-BGC and PnET-II were similar in a number of other respects. MOD17 was part of the NASA Earth Observation System program and was the first satellite-driven dataset to monitor continuous vegetation productivity on a global scale (Zhao et al. 2005). GPP estimates from both BigFoot and MODIS together provided a means of landscape comparison with our PnET-II GPP estimates. To match our canopy %N_e remote-sensing acquisition, we only used 2003 GPP results from BigFoot (Turner et al. 2006b) and MOD17 (version 5.1).

Results

Model prediction and validation

PnET-II-predicted GPP was extracted for a 250-m footprint around the two flux towers, EMS and HEM, and compared to tower-derived GPP. In general, model predictions corresponded reasonably well with measured monthly values (Fig. 1). The r^2 of predicted versus observed values during the growing season at EMS and HEM were 0.82 ($p < 0.001$) and 0.79 ($p < 0.001$), respectively (Supplementary Fig. S6). The overall data pooled for the two sites had an r^2 of 0.80 ($p < 0.001$). Although predicted monthly GPP accounted for similar amount of variance of observations at both EMS and HEM, GPP at EMS was overestimated in the early growing season when observed GPP was ranged from 100 to 200 g C m^{-2} month^{-1} (May), and underestimated in the late growing season when observed GPP was greater than 300 g C m^{-2} month^{-1} (July and August). Predicted annual GPPs at EMS and HEM were 1440.0 ± 100.2 and 1268.8 ± 58.2 g C m^{-2} year^{-1}, compared with 1525.7 ± 228.9 and 1330.9 ± 169.2 g C m^{-2} year^{-1} from the flux towers, respectively.

We assessed the relationship between ANPP and canopy %N_f, both collected over a series of plots in the BigFoot study area, to examine the spatial correlation of
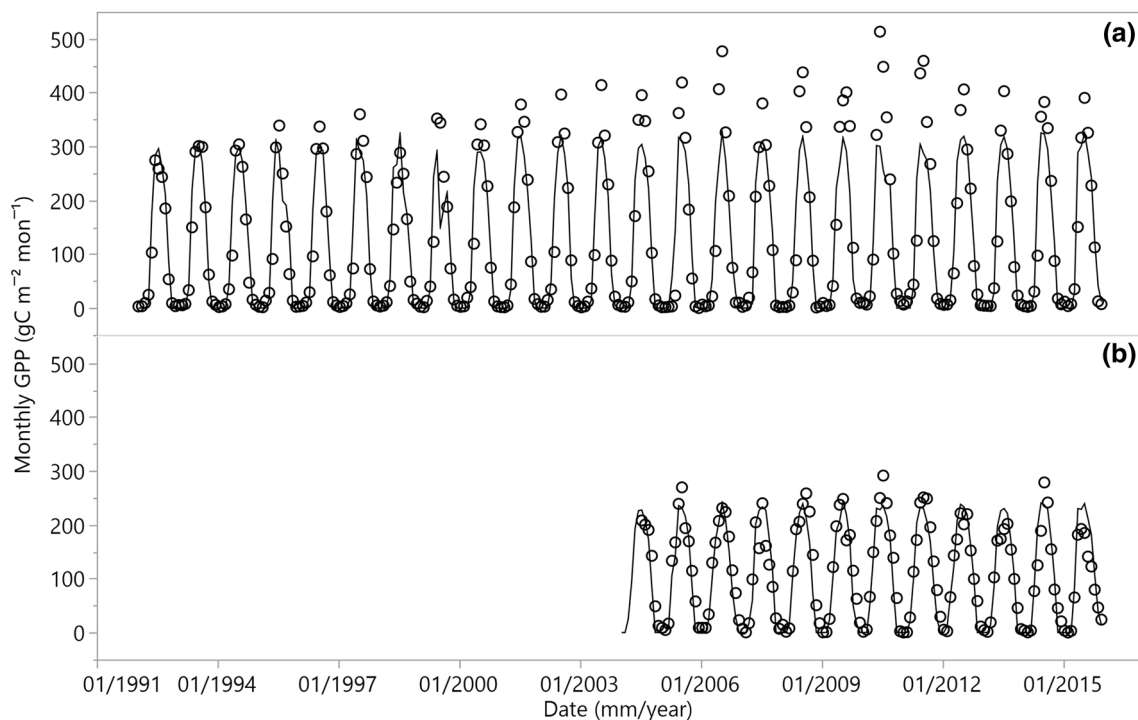

Fig. 1 Predicted versus observed monthly GPPs at towers **a** EMS and **b** HEM. The open circles denote tower monthly GPP, and solid line for predicted GPP. The r^2 of predicted versus observed values during the growing season (April–November) at EMS and HEM were 0.82 ($p < 0.001$) and 0.79 ($p < 0.001$) with RMSE of 47.3 and 36.0 g C m^{-2} month^{-1}, respectively

canopy %N with carbon assimilation. Observed canopy %N_f was significantly positively correlated to observed ANPP ($r^2 = 0.48$; $p < 0.001$; Fig. 2a). Larger residuals of predicted values occurred at the higher end of canopy %N_f. Although LAI can be an important productivity indicator across biomes (Reich 2012), the measured ANPP did not show a significant correlation with measured LAI at HF ($r^2 = 0.11$; $p < 0.16$; Fig. 2b).
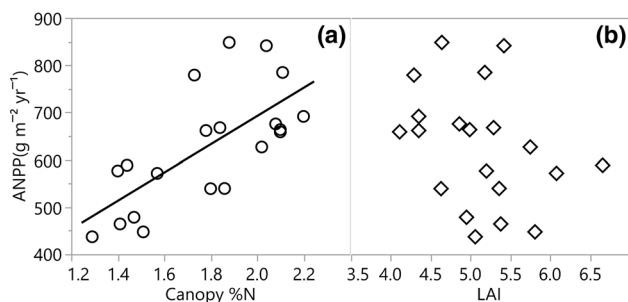

Fig. 2 Observed aboveground net primary production (ANPP) versus observed **a** canopy %N and **b** leaf area index (LAI) at HF. Canopy %N explained 48% of the variance in ANPP ($r^2 = 0.48$; $p < 0.001$), and LAI only explained 11% ($r^2 = 0.11$; $p < 0.16$)

Spatial patterns of canopy %N and GPP

Remotely sensed canopy %N_e ranged from 0.5 to 2.9 with a mean of 1.75 across the study region. The coefficient of variation was 14.3% (Figs. 3, 4a). While patterns of GPP predicted by PnET-II were similar to those for canopy %N_e, GPP was less variable over the study area than canopy %N_e, with values ranging from 797 to 1622 g C m^{-2} year^{-1}, a mean of 1324 g C m^{-2} year^{-1}, and a coefficient of variation of 6% (Figs. 3, 4c). No significant relationships were observed between canopy %N_e or GPP and slope, aspect, and climate variables including temperature, precipitation, and PAR. This is not surprising given the small size and lack of topographic complexity of HF. After we had detrended annual GPP with canopy %N_e, the residual of GPP was significantly positively correlated to average PAR during the whole growing season ($r^2 = 0.69$; $p < 0.001$; data not shown).

At the landscape scale, predicted GPP was positively and linearly correlated to canopy %N_e ($r^2 = 0.97$; $p < 0.001$; Fig. 4b). Deciduous species with higher canopy %N_e (Wright et al. 2004) and higher light use efficiency (Ollinger et al. 2008) occur at the higher end of GPP while evergreens occur at the lower end. It is noted that within the range of canopy %N_e (i.e., 0.94–2.3, where both deciduous and evergreen species exist) predicted GPP of deciduous and evergreen stands can be similar (Fig. 4d) because the longer growing
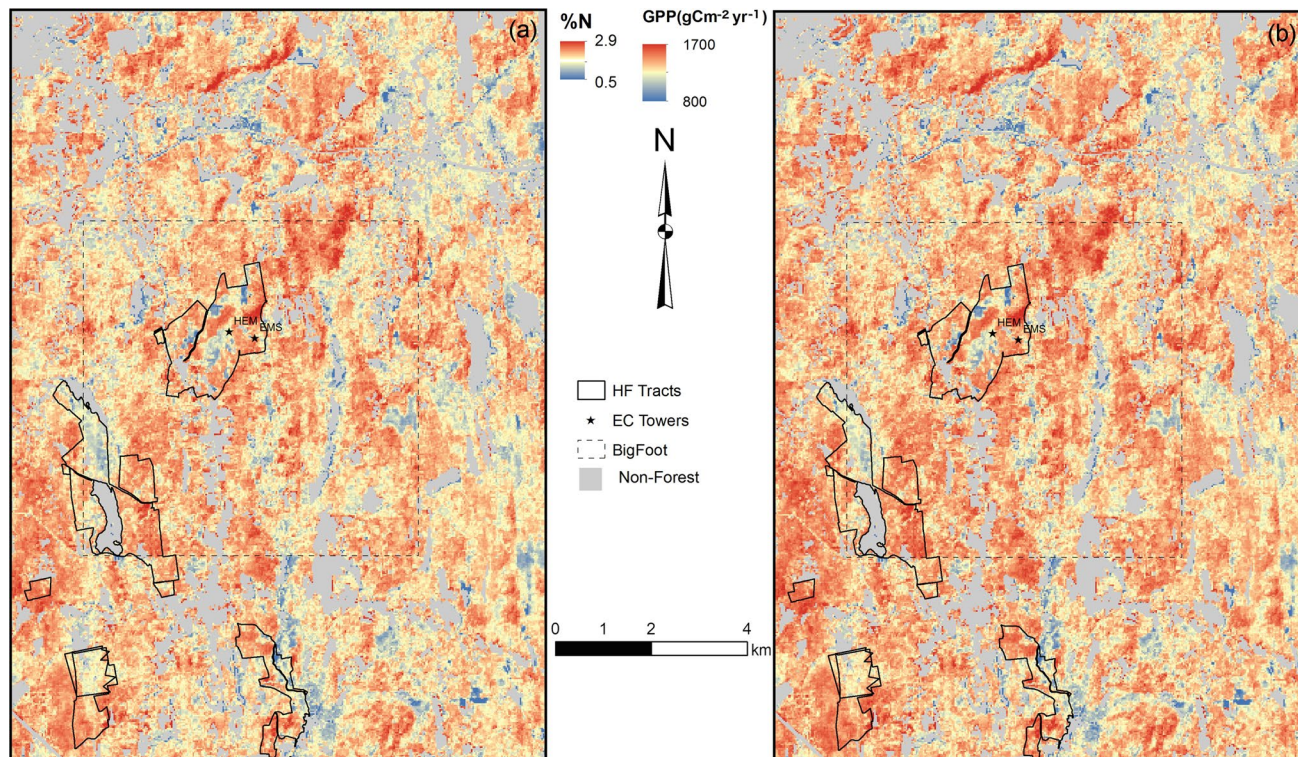

Fig. 3 Spatial patterns in **a** AVIRIS remotely sensed canopy %N and **b** PnET-II modeled GPP. This figure appears in color in the online version of the journal
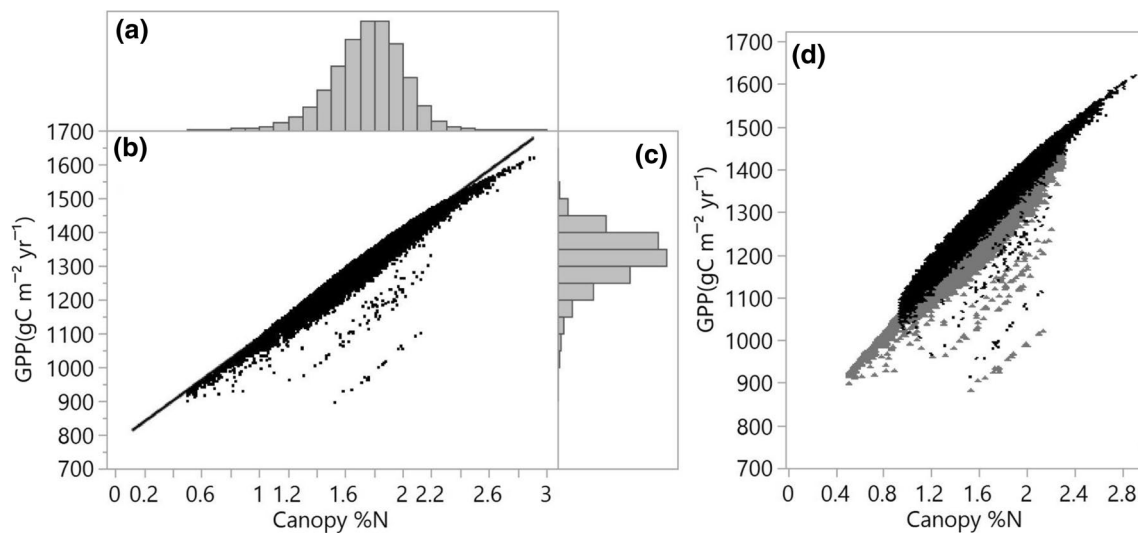
Fig. 4 Relationships between remotely sensed canopy %N and PnET-II modeled GPP, **a** distribution of canopy %N ($n = 16,5301$), **b** relationship between canopy %N and GPP for all grids weighted by the fraction of deciduous and evergreen stands (GPP = 309.6 × Canopy %N + 783.6; $r^2 = 0.97$; $p < 0.001$), **c** distribution of GPP ($n = 165,301$), and **d** GPP components for pure deciduous and evergreen in pixels associated with the lumped canopy %N. Black dots in figure d represent deciduous stands and gray triangles the evergreen stands

season of evergreen stands can at least partially compensate for their lower midsummer photosynthetic capacity.

Relationships with forest composition, land-use history, and soil drainage

Spatial patterns of canopy $\%N_e$ and predicted GPP broadly reflected the distribution of functional types (Fig. 5a, b, $p < 0.01$). It should be noted, however, that variation in canopy $\%N_e$ was driven by both the deciduous/evergreen ratio as well as the variation in %N within each forest type (Supplementary Fig. S4). The highest canopy $\%N_e$ and GPP occurred in hardwood (deciduous) stands (mean values were 1.91 and 1373.9 g C m^{-2} year^{-1}, respectively), and the lowest canopy $\%N_e$ and GPP occurred in needle-leaved evergreens (mean values were 1.46 and 1247.9 g C m^{-2} year^{-1}, respectively), with mean canopy $\%N_e$ and GPP for mixed forests falling between those for deciduous and evergreen stands (mean %N 1.73, mean GPP 1321.4 g C m^{-2} year^{-1}; Fig. 5a, b).

Canopy $\%N_e$ and predicted GPP differed significantly across the land-use history categories included in the Prospect Hill Tract land-use coverage ($p < 0.05$; Fig. 5c, d). Stands that had been used as woodlots had the lowest canopy $\%N_e$ and GPP (1.60 and 1272.8 g C m^{-2} year^{-1}, respectively). Stands with a history of unimproved pasture had the highest canopy $\%N_e$ and GPP (1.84 and 1349.2 g C m^{-2} year^{-1}, respectively). Relatively fertile soils with a history of cultivated agriculture and improved pasture had intermediate canopy $\%N_e$ and GPP, with higher values in cultivated lands than in improved pasture.

From examining relationships between soil drainage classes and canopy $\%N_e$ and GPP, we found that both canopy $\%N_e$ and GPP were lowest in stands with the driest soils (e.g., drainage class D1, with 1.6 mean canopy $\%N_e$ and 1330 g C m^{-2} year^{-1} GPP) and the wettest soils (e.g., drainage class D6, with canopy $\%N_e$ and GPP of 1.46 and 1241.5 g C m^{-2} year^{-1}; Fig. 5e, f). This pattern was related to forest composition. Lower values of canopy $\%N_e$ and GPP were associated with the higher fraction of evergreen stands (Fig. 5f); e.g., peat soils were dominated by hemlock and spruce in the southwest of HEM tower, and white pine, red oak, and hemlock were dominant species on the driest soils (Fig. 5f).

Comparisons of predicted GPP with BigFoot and MODIS estimates

Mapped GPP estimates from BigFoot and MODIS were compared to estimates generated with PnET-II to illustrate their similarities. When compared with seasonal patterns of GPP, PnET-II GPP was more in line with MODIS than with BigFoot (Fig. 6a). However, the spatial distribution of annual GPP from this study and BigFoot were more similar than MODIS (Supplementary Fig. S7) as they had similar spatial resolutions. PnET-II annual GPP in the BigFoot area (1248.0 ± 91.0 g C m^{-2} year^{-1}) was closer to that from BigFoot (1250.1 ± 361.4 g C m^{-2} year^{-1}) than from MODIS (1401.0 ± 79.0 g C m^{-2} year^{-1}).

Because BigFoot's Biome-BGC productivity estimates were driven by spatial patterns in remotely sensed LAI (Turner et al. 2004), which was not well correlated with
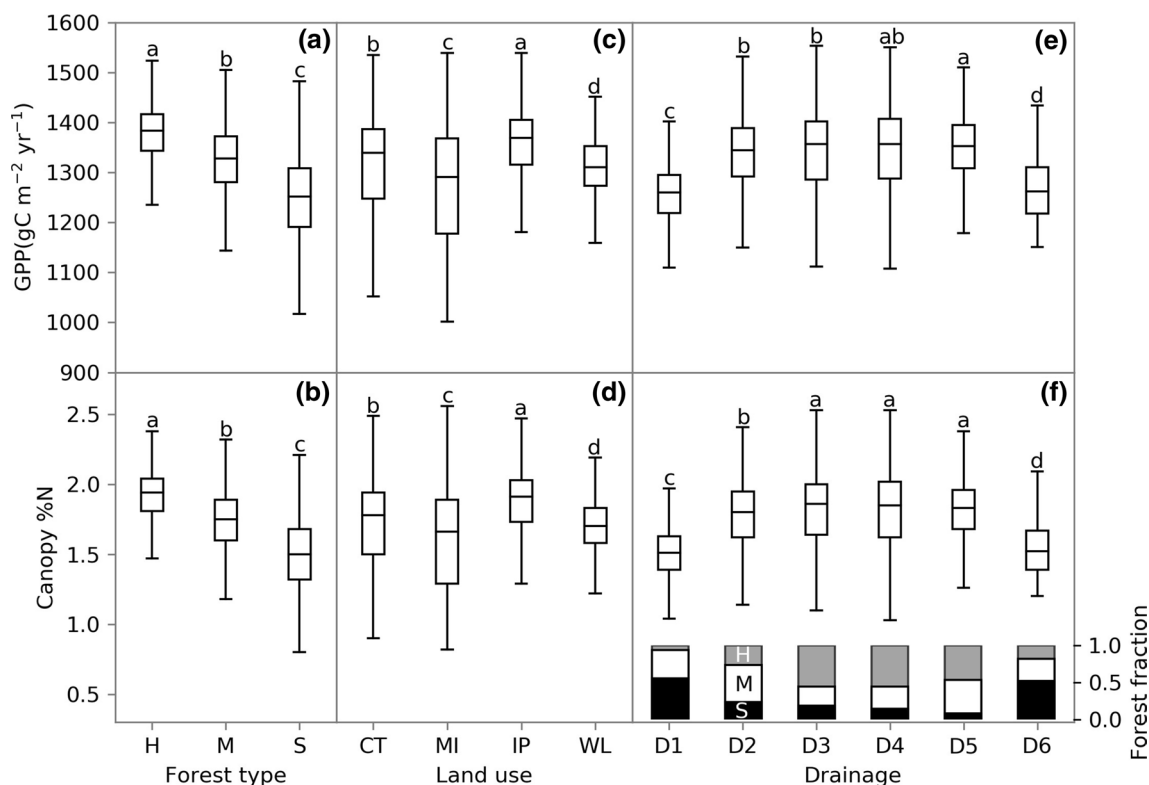
Fig. 5 Relationships between annual GPP, canopy %N and (**a**, **b**) forest type, (**c**, **d**) land-use history in Prospect Hill Tract, and (**e**, **f**) soil drainage. H, S, and M stand for hardwood ($n=4213$), softwood ($n=1651$), and mixed stands ($n=3045$) in figures **a**, **b**. CT represents historically cultivated land use ($n=232$), IP mowed or improved pasture ($n=580$), UP unimproved pasture ($n=2247$), and WL woodlot ($n=505$). Drainage classes increase in moisture with increasing class number, where D1 is excessively drained ($n=405$ with H 26, S 223, and M 156), D2 is somewhat excessively drained ($n=1525$ with H 402, S 352, and M 771), D3 is well drained ($n=3562$ with H 1989, S 648, and M 925), D4 is moderately well drained ($n=1025$ with H 575, S 150, and M 300), D5 is very poorly drained ($n=1153$ with H 538, S 90, and M 525), and D6 is peat ($n=202$ with H 37, S 104, and M 61). The bars in figure **f** indicate forest composition (H, S, and M) in soil drainage classes. Different lower case letters on each box in each panel represent statistically significant differences in the mean among groups in the same panel ($p<0.05$)

ANPP at HF (Fig. 2b), we viewed spatial patterns in productivity predicted by PnET-II and canopy %N_e as being more reliable. Compared with PnET-II annual estimates degraded to 1 km MODIS resolution, MODIS annual GPP was greater by 12.3% in this study area. The ratio of MODIS annual GPP to PnET-II annual GPP on each MODIS pixel, reflecting the difference between MODIS and PnET-II estimates, was negatively correlated to canopy %N_e (Fig. 6b).

Discussion

Uncertainties in predicted GPP

For the time period of our model validation, EMS tower data showed a trend of increasing GPP over time ($r^2=0.74$; $p<0.01$), especially after the year 2000. While PnET-II mostly underestimated values of summer GPP during this period (Fig. 1a), variation in GPP on a monthly timescale

nevertheless reflected responses to the environment. The PnET-II model underestimated the average annual values of GPP (1440.0 versus 1525.7 g C m^{-2} year^{-1}) by 5.6%. The underestimation was about 9.8% after the year 2000. The increase in annual GPP at the EMS site has been, in part, attributed to parallel increases in midsummer photosynthetic capacity at the high light level, peak leaf area index (Urbanski et al. 2007), water-use efficiency (Keenan et al. 2013; Belmecheri et al. 2014), and CO_2 fertilization (Urbanski et al. 2007). However, factors mentioned above have not yet fully explained the observed trend. The underlying reason is still elusive. Meanwhile, the increase in the past few years seems to have gone away, also for reasons that are not clear. PnET-II predicted GPP showed a slightly increasing trend ($r^2=0.57$; $p<0.01$) due to an increased ambient atmospheric CO_2 concentration which led to enhanced photosynthesis and water-use efficiency (Ollinger et al. 2002a). Because additional mechanisms explaining the trend of increasing tower GPP have not yet been identified and thus not
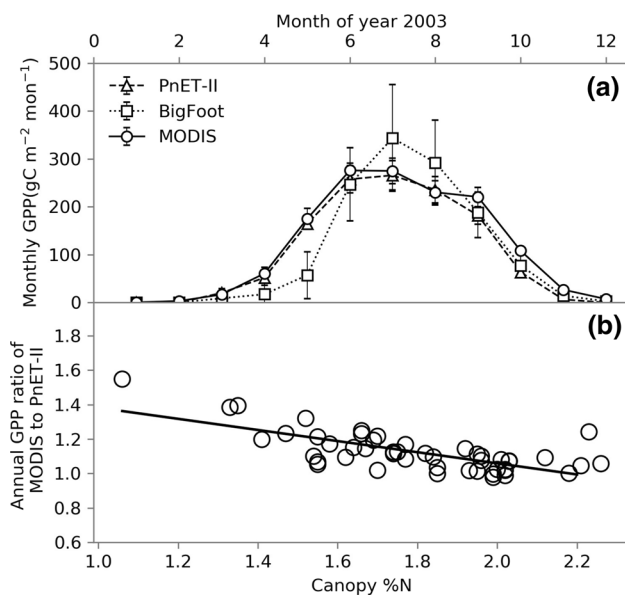
Fig. 6 Comparisons of estimated GPP in 2003 among PnET-II, Big-Foot, and MODIS, **a** seasonal patterns of estimated monthly GPP, **b** ratios of annual MODIS GPP to PnET-II GPP in MODIS pixels in relation to remotely sensed canopy %N ($GPP_{MODIS}/GPP_{PnET} = -0.32 \times Canopy\ \%N + 1.70$; $r^2 = 0.52$; $p < 0.001$). The vertical bars in figure a represent a standard deviation within a 7×7-km region

represented in PnET-II modeling, the uncertainty of their impacts to the PnET-II-predicted spatial patterns is hard to assess.

Tower GPP at HEM site showed a decline after the year 2011 due to the invasive hemlock woolly adelgid (*Adelges tsugae*) that caused foliar damage, crown loss, and mortality of host trees (Orwig et al. 2012). The absence of woolly adelgid infestation in the model likely contributed to the underestimation (by 8.9%) of predicted GPP.

Relationships with forest composition, land-use history, and soil drainage

Landscape scale remotely sensed canopy $\%N_e$ was spatially related to a combination of forest composition and variation in foliar %N within individual forest types, both of which were influenced by soil drainage and land-use history at HF. As deciduous and evergreen forests have contrasting foliar %N (Wright et al. 2004), canopy $\%N_e$ can broadly reflect information about forest composition in mixed forest (Martin et al. 1998). The ability to capture this component of variation in stand-level canopy %N is not trivial given the challenge of estimating sub-pixel variation in forest composition.

At HF, forest composition was influenced by historical factors (primary versus secondary woodlands, forest age, cutting history and timing of site abandonment) and site factors (slope position and soil drainage; Foster 1992).

The relationship between canopy $\%N_e$ and soil drainage (Fig. 5f), as well as land-use history (Fig. 5d), reflected the relationship between canopy $\%N_e$ and forest composition. The land-use pattern of HF in the mid-1800s, including woodlot (13%), tilled fields (16%), pasture (70%) and marsh (1%), correlated with soil drainage and proximity to farmhouses and town roads (Foster 1992). Field abandonment and reforestation after the 1850s proceeded outward from poorly drained pasture adjacent to woodlots and finally included productive tilled land. Woodlots often occupied steep and rocky slopes, wetlands or narrow valleys in infertile soils, which may explain why those areas are lower in present-day mean canopy $\%N_e$. A lower hardwood fraction (17.6%) occurred in woodlots than that in cultivated (43.3%), improved (43.8%), and unimproved soils (63.8%). Higher canopy $\%N_e$ in soils with a history of unimproved pasture (Fig. 5d) might be attributed to the earlier abandonment dates and thus longer recovery periods (Hooker and Compton 2003). The fact that gray birch (*Betula populifolia*), poplar (*Populus* spp.), and red maple were most abundant in old-cultivated fields could also lead to higher canopy $\%N_e$ than that in old-improved pasture lands, which white pine and American chestnut (*Castanea dentata*) were largely confined to (Fig. 5d). The combined influence of agricultural use, soil fertility, and recovery period likely led to the complicated canopy $\%N_e$ patterns.

Relationships between canopy %N and GPP

In this study, remotely sensed canopy $\%N_e$ was strongly related to GPP predicted by PnET-II (Fig. 4b). This result emerges in the context that the landscape at HF consists closed canopy forest with relatively high LAI (4.9 $m^2\ m^{-2}$) and near-complete interception of available light. The relationship reflects the well-established relationship between leaf-level photosynthetic capacity and foliar N concentrations (Evans 1989; Reich et al. 1999a; Wright et al. 2004) and provides further support that leaf level trends scale over whole-plant canopies in high LAI systems (Ollinger et al. 2008). Although predicted GPP was only validated at two sites (EMS and HEM), the relationship between field-measured ANPP and canopy $\%N_f$ and the fact that ANPP and GPP are strongly related in forests, more generally (Litton et al. 2007), support the prediction that landscape-scale spatial patterns of C assimilation follow patterns of canopy $\%N_e$. This result is also in line with the NPP–canopy $\%N_f$ relationships across a wide range of plant species and functional groups, reported by Smith et al. (2002) and Reich (2012).

Although deciduous species generally have greater photosynthetic potential per unit of leaf mass than evergreen, they often have less leaf mass per leaf area, shorter leaf lifespan (Wright et al. 2004), and therefore less total

displayed foliage biomass. The combined effect of foliar %N and foliage biomass could make GPP for each species comparable in the mixed stands (Fig. 4d). When N availability limits growth in mixed forests, deciduous and evergreen species show a trend of coordination in term of abundance and canopy nitrogen concentration (Dybzinski et al. 2013). Greater deciduous $\%N_f$ is associated with greater evergreen $\%N_f$, but less fraction of evergreen (see Supplementary Figs. S3, S4). This co-varying features may reflect the site quality and soil N availability (Ollinger et al. 2002b), and their effects on carbon assimilation is worth more study. Using lumped canopy %N (e.g., AVIRIS $\%N_e$) may provide a generalized approach to estimating carbon assimilation over time and space.

The result that MODIS GPP was greater than GPP estimates from PnET-II is consistent with results from Turner et al. (2006a), who reported that MODIS tended to overestimate GPP at HF. In a landscape where climate variation is small, errors in MODIS GPP stems from either the fraction of photosynthetically active radiation absorbed by the canopy (FPAR) or the vegetation light use efficiency (LUEmax) in MODIS GPP algorithm. For our study area, a closed canopy forest with relatively high LAI and near-complete interception of available light, LUEmax, therefore, could be a significant source of error. The MODIS GPP algorithm determines LUEmax based on land cover classes; e.g., in our study, MODIS categorized land covers as mixed forests and deciduous forests only, each of which had a fixed LUEmax. Previous studies demonstrated that light-use efficiency was positively related to foliar $\%N_f$ (Green et al. 2003; Kergoat et al. 2008; Ollinger et al. 2008). Given the wide range of canopy $\%N_e$ in our study area (Figs. 3, 4c), the errors of LUEmax associated with canopy %N in this study could be a major factor contributing to the difference between MODIS GPP and PnET-II GPP (Fig. 6b). With the distinct foliar %N and light-use efficiency for evergreen and deciduous stands, mix forests could lead to a factor of 2 of variation in canopy %N, and consequently, light-use efficiency. A fixed LUEmax for all mixed forests globally, as employed by the MODIS GPP algorithm (1.051 g C m^{-2} day^{-1} MJ^{-1}), could introduce considerable uncertainties in GPP estimates in mixed forests with a range of fraction of evergreen and deciduous species, which may be considerably reduced by canopy %N-dependent LUEmax. In that perspective, the link between canopy %N and canopy reflectance in the near infrared (800–850 nm) in temperate and boreal forests (Ollinger et al. 2008; Lepine et al. 2016), i.e., canopy $\%N_e$ remote sensing, may provide the means for a straightforward and efficient approach to scaling canopy nitrogen via broadband satellite data to broad-scale productivity estimates, such as MODIS GPP and NPP products.

Conclusions

At Harvard Forest and its surrounding area, landscape-scale canopy %N, spatially mapped using high spectral resolution remote sensing, was demonstrated to relate to forest composition, soil drainage, and land-use history. Mapped canopy $\%N_e$ was positively correlated with the relative fraction of deciduous and evergreen species in the stands as well as to variation in foliar $\%N_f$ within each type. Land-use legacies were evident in the present-day canopy $\%N_e$ although some of this likely reflect pre-existing conditions that led to some areas being used for specific purposes. Woodlots had the lowest canopy $\%N_e$ and stands in old unimproved pasture had the highest values, followed by stands historically cultivated and improved for pasture. Integration of remotely sensed canopy $\%N_e$ to the ecosystem process model, PnET-II, demonstrated that canopy $\%N_e$ regulated the forest canopy GPP, with both GPP and canopy $\%N_e$ showing similar relationships with forest composition, soil drainage, and land-use history. The comparison of PnET-II GPP with Big-Foot and MODIS GPP indicated that canopy $\%N_e$ explained much of the difference between MODIS GPP and PnET-II GPP, suggesting that global MODIS GPP estimates may be improved if broad-scale estimates of canopy $\%N_e$ become available.

References

Aber JD, Driscoll CT (1997) Effects of land use, climate variation, and N deposition on N cycling and C storage in northern hardwood forests. Glob Biogeochem Cycles 11:639–648. https://doi.org/10.1029/97GB01366

Aber JD, Ollinger SV, Federer CA et al (1995) Predicting the effects of climate change on water yield and forest production in the northeastern United States. Clim Res 5:207–222. https://doi.org/10.3354/cr005207

Aber JD, Ollinger SV, Driscoll CT (1997) Modeling nitrogen saturation in forest ecosystems in response to land use and atmospheric deposition. Ecol Model 101:61–78. https://doi.org/10.1016/S0304-3800(97)01953-4

Belmecheri S, Maxwell RS, Taylor AH et al (2014) Tree-ring δ13C tracks flux tower ecosystem productivity estimates in a NE temperate forest. Environ Res Lett 9:074011. https://doi.org/10.1088/1748-9326/9/7/074011

BigFoot (2005) http://www.fsl.orst.edu/larse/bigfoot/index.html

Dybzinski R, Farrior CE, Ollinger S, Pacala SW (2013) Interspecific vs intraspecific patterns in leaf nitrogen of forest trees across nitrogen availability gradients. New Phytol 200:112–121. https://doi.org/10.1111/nph.12353

Evans JR (1989) Photosynthesis and nitrogen relationships in leaves of C_3 plants. Oecologia 78:9–19

Foster DR (1988) Species and stand response to catastrophic wind in Central New England, USA. J Ecol 76:135–151. https://doi.org/10.2307/2260458

Foster DR (1992) Land-use history (1730–1990) and vegetation dynamics in Central New England, USA. J Ecol 80:753–771. https://doi.org/10.2307/2260864

Foster DR, Aber JD, Melillo JM et al (1997) Forest response to disturbance and anthropogenic stress. Bioscience 47:437–445. https://doi.org/10.2307/1313059

Galloway JN, Dentener FJ, Capone DG et al (2004) Nitrogen cycles: past, present, and future. Biogeochemistry 70:153–226. https://doi.org/10.1007/s10533-004-0370-0

Goodale CL, Aber JD (2001) The long-term effects of land-use history on nitrogen cycling in Northern Hardwood Forests. Ecol Appl 11:253–267. https://doi.org/10.2307/3061071

Green DS, Erickson JE, Kruger EL (2003) Foliar morphology and canopy nitrogen as predictors of light-use efficiency in terrestrial vegetation. Agric For Meteorol 115:163–171. https://doi.org/10.1016/S0168-1923(02)00210-1

Hall B (2005) Historical GIS data for Harvard Forest properties from 1908 to Present. Harvard Forest Data Archive: HF110

Hooker TD, Compton JE (2003) Forest ecosystem carbon and nitrogen accumulation during the first century after agricultural abandonment. Ecol Appl 13:PLS 9–PLS 13. https://doi.org/10.1890/1051-0761(2003)013[0299:fecana]2.0.co;2

Keenan TF, Hollinger DY, Bohrer G et al (2013) Increase in forest water-use efficiency as atmospheric carbon dioxide concentrations rise. Nature 499:324–327. https://doi.org/10.1038/nature12291

Kergoat L, Lafont S, Arneth A et al (2008) Nitrogen controls plant canopy light-use efficiency in temperate and boreal ecosystems. J Geophys Res 113:G04017. https://doi.org/10.1029/2007JG000676

LeBauer DS, Treseder KK (2008) Nitrogen limitation of net primary productivity in terrestrial ecosystems is globally distributed. Ecology 89:371–379. https://doi.org/10.1890/06-2057.1

Lepine LC, Ollinger SV, Ouimette AP, Martin ME (2016) Examining spectral reflectance features related to foliar nitrogen in forests: implications for broad-scale nitrogen mapping. Remote Sens Environ 173:174–186. https://doi.org/10.1016/j.rse.2015.11.028

Litton CM, Raich JW, Ryan MG (2007) Carbon allocation in forest ecosystems. Glob Change Biol 13:2089–2109. https://doi.org/10.1111/j.1365-2486.2007.01420.x

Martin ME, Newman SD, Aber JD, Congalton RG (1998) Determining forest species composition using high spectral resolution remote sensing data. Remote Sens Environ 65:249–254. https://doi.org/10.1016/S0034-4257(98)00035-2

Martin ME, Plourde LC, Ollinger SV et al (2008) A generalizable method for remote sensing of canopy nitrogen across a wide range of forest ecosystems. Remote Sens Environ 112:3511–3519. https://doi.org/10.1016/j.rse.2008.04.008

McNeil BE, Read JM, Driscoll CT (2007) Foliar nitrogen responses to elevated atmospheric nitrogen deposition in nine temperate forest canopy species. Environ Sci Technol 41:5191–5197. https://doi.org/10.1021/es062901z

McNulty SG (2002) Hurricane impacts on US forest carbon sequestration. Environ Pollut 116(Supplement 1):S17–S24. https://doi.org/10.1016/S0269-7491(01)00242-1

Merilä P, Derome J (2008) Relationships between needle nutrient composition in Scots pine and Norway spruce stands and the respective concentrations in the organic layer and in percolation water. Boreal Environ Res 13:35–47

Munger W, Hadley J (2003) Net carbon exchange of an old-growth Hemlock Forest at Harvard Forest HEM Tower since 2000. Harvard Forest Data Archive: HF103

Munger W, Wofsy S (1999) Canopy-atmosphere exchange of carbon, water and energy at Harvard Forest EMS Tower since 1991. Harvard Forest Data Archive: HF004

Ollinger SV (2011) Sources of variability in canopy reflectance and the convergent properties of plants. New Phytol 189:375–394. https://doi.org/10.1111/j.1469-8137.2010.03536.x

Ollinger SV, Smith M-L (2005) Net primary production and canopy nitrogen in a temperate forest landscape: an analysis using imaging spectroscopy, modeling and field data. Ecosystems 8:760–778. https://doi.org/10.1007/s10021-005-0079-5

Ollinger SV, Aber JD, Reich PB, Freuder RJ (2002a) Interactive effects of nitrogen deposition, tropospheric ozone, elevated CO_2 and land use history on the carbon dynamics of northern hardwood forests. Glob Change Biol 8:545–562. https://doi.org/10.1046/j.1365-2486.2002.00482.x

Ollinger SV, Smith ML, Martin ME et al (2002b) Regional variation in foliar chemistry and n cycling among forests of diverse history and composition. Ecology 83:339–355. https://doi.org/10.1890/0012-9658(2002)083[0339:RVIFCA]2.0.CO;2

Ollinger SV, Richardson AD, Martin ME et al (2008) Canopy nitrogen, carbon assimilation, and albedo in temperate and boreal forests: functional relations and potential climate feedbacks. PNAS 105:19336–19341. https://doi.org/10.1073/pnas.0810021105

Orwig DA, Thompson JR, Povak NA et al (2012) A foundation tree at the precipice: *Tsuga canadensis* health after the arrival of *Adelges tsugae* in central New England. Ecosphere 3:1–16. https://doi.org/10.1890/ES11-0277.1

Parton W, Silver WL, Burke IC et al (2007) Global-scale similarities in nitrogen release patterns during long-term decomposition. Science 315:361–364. https://doi.org/10.1126/science.1134853

Reich PB (2012) Key canopy traits drive forest productivity. Proc R Soc Lond B Biol Sci. https://doi.org/10.1098/rspb.2011.2270

Reich PB, Ellsworth DS, Walters MB et al (1999a) Generality of leaf trait relationships: a test across six biomes. Ecology 80:1955–1969. https://doi.org/10.1890/0012-9658(1999)080[1955:GOLTRA]2.0.CO;2

Reich PB, Turner DP, Bolstad P (1999b) An approach to spatially distributed modeling of net primary production (NPP) at the landscape scale and its application in validation of EOS NPP products. Remote Sens Environ 70:69–81. https://doi.org/10.1016/S0034-4257(99)00058-9

Reich PB, Tjoelker MG, Pregitzer KS et al (2008) Scaling of respiration to nitrogen in leaves, stems and roots of higher land plants. Ecol Lett 11:793–801. https://doi.org/10.1111/j.1461-0248.2008.01185.x

Reichstein M, Falge E, Baldocchi D et al (2005) On the separation of net ecosystem exchange into assimilation and ecosystem respiration: review and improved algorithm. Glob Change Biol 11:1424–1439. https://doi.org/10.1111/j.1365-2486.2005.001002.x

Running SW, Nemani RR, Heinsch FA et al (2004) A continuous satellite-derived measure of global terrestrial primary production. Bioscience 54:547–560. https://doi.org/10.1641/0006-3568(2004)054[0547:ACSMOG]2.0.CO;2

Smith M-L, Martin ME (2001) A plot-based method for rapid estimation of forest canopy chemistry. Can J For Res 31:549–555. https://doi.org/10.1139/x00-187

Smith M-L, Ollinger SV, Martin ME et al (2002) Direct estimation of aboveground forest productivity through hyperspectral remote sensing of canopy nitrogen. Ecol Appl 12:1286–1302. https://doi.org/10.1890/1051-0761(2002)012[1286:DEOAFP]2.0.CO;2

Smith M-L, Martin ME, Plourde L, Ollinger SV (2003) Analysis of hyperspectral data for estimation of temperate forest canopy nitrogen concentration: comparison between an airborne (AVIRIS) and a spaceborne (Hyperion) sensor. IEEE Trans Geosci Remote Sens 41:1332–1337. https://doi.org/10.1109/TGRS.2003.813128

Thornton PE, Running SW (1999) An improved algorithm for estimating incident daily solar radiation from measurements of temperature, humidity, and precipitation. Agric For Meteorol 93:211–228. https://doi.org/10.1016/S0168-1923(98)00126-9

Thornton PE, Running SW, White MA (1997) Generating surfaces of daily meteorological variables over large regions of complex terrain. J Hydrol 190:214–251. https://doi.org/10.1016/S0022-1694(96)03128-9

Turner DP, Ollinger S, Smith M et al (2004) Scaling net primary production to a MODIS footprint in support of Earth observing system product validation. Int J Remote Sens 25:1961–1979. https://doi.org/10.1080/0143116031000150013

Turner DP, Ritts WD, Cohen WB et al (2006a) Evaluation of MODIS NPP and GPP products across multiple biomes. Remote Sens Environ 102:282–292. https://doi.org/10.1016/j.rse.2006.02.017

Turner DP, Ritts WD, Gregory MJ (2006b) BIGFOOT GPP surfaces for north and south American sites, 2000–2004. Data set. http://www.daac.ornl.gov from Oak Ridge National Laboratory Distributed Active Archive Center, Oak Ridge, Tennessee, USA. https://doi.org/10.3334/ornldaac/749

Urbanski S, Barford C, Wofsy S et al (2007) Factors controlling CO_2 exchange on timescales from hourly to decadal at Harvard Forest. J Geophys Res 112:G02020. https://doi.org/10.1029/2006JG000293

Weishampel JF, Drake JB, Cooper A et al (2007) Forest canopy recovery from the 1938 hurricane and subsequent salvage damage measured with airborne LiDAR. Remote Sens Environ 109:142–153. https://doi.org/10.1016/j.rse.2006.12.016

Wright IJ, Reich PB, Westoby M et al (2004) The worldwide leaf economics spectrum. Nature 428:821–827. https://doi.org/10.1038/nature02403

Zhao M, Heinsch FA, Nemani RR, Running SW (2005) Improvements of the MODIS terrestrial gross and net primary production global data set. Remote Sens Environ 95:164–176. https://doi.org/10.1016/j.rse.2004.12.011